Marine and Petroleum Geology 110 (2019) 886–900

Contents lists available at ScienceDirect

Marine and Petroleum Geology

journal homepage: www.elsevier.com/locate/marpetgeo

Research paper

Mineralogy and inorganic geochemistry of the Es_4 shales of the Damintun Sag, northeast of the Bohai Bay Basin: Implication for depositional environment

Hongxia Li[a], Bo Liu[a,*], Xingzhou Liu[b], Lina Meng[c], Lijuan Cheng[a], Haixue Wang[d]

[a] Key Laboratory of Continental Shale Hydrocarbon Accumulation and Efficient Development (Northeast Petroleum University), Ministry of Education, Daqing 163318, PR China
[b] PetroChina Liaohe Oilfield Company, Panjin 124000, PR China
[c] PetroChina Dagang Oilfield Company, Tianjin 300280, PR China
[d] Laboratory of CNPC Fault Controlling Reservoir, Northeast Petroleum University, Daqing 163318, PR China

ARTICLE INFO

Keywords:
Inorganic geochemistry
The Es_4 shales
Provenance
Tectonic setting
Depositional environment
The Damintun Sag

ABSTRACT

The Es_4 shale, namely the fourth member of the Shahejie Formation deposited during the Eocene, is one of the most important hydrocarbon source rocks widely distributed in the Bohai Bay Basin. Twenty-nine samples with TOC ranging from 1.59% to 7.50% were gathered from the Es_4 shale at the Damintun Sag. Compositions of mineralogy, major oxides, trace elements and REEs were analyzed to study their provenance, paleo-environment and tectonic setting. The Es_4 shales show $(La/Yb)_N$ ratios ranging from 10.98 to 14.24 with an average of 12.45, and have similar C1-chondrite normalized REE + Y distribution to intermediate ~ mafic igneous rocks developed at the northeast NCC (North China Craton) during the Mesozoic and the Cenozoic. Weight ratios of Al_2O_3/TiO_2, TiO_2/Zr and Cr/Th of the Es_4 shales show values of 12.76–18.81, 71.2–147.8 and 12.96–19.91, which reveal a common source of detritus from intermediate igneous rocks. The Es_4 shales present values of K_2O/Al_2O_3, ICV (Index of Compositional Variability), PIA (Plagioclase Index of Alteration) and CIA (Chemical Index of Alteration) locating at 0.07–0.21, 0.80–2.04, 39.82–83.85 and 44.76–76.15, respectively. These weathering proxies imply that the Es_4 shales underwent moderate to intense weathering. Sensitive redox indicators, pyrite (1.7% ~ 12.6%) and TOC (1.59% ~ 7.50%), indicate a reduced depositional condition. TOC of the Es_4 shales is positively correlated with U/Th and negatively correlated with $(La/Yb)_N$, which indicates that organic matters were largely preserved at more reduced conditions and could be diluted by detritus influx. Absolute ratios of U/Th (0.11–0.25), V/Cr (0.80–1.46) and Ni/Co (2.42–4.40) suggested an oxic environment, which is contrary to the conclusion supported by high TOC content and existence of pyrite. These absolute ratios of U/Th, V/Cr and Ni/Co are probably inherited from parental rocks rather than reflecting redox conditions in this study. Shale samples showing higher TOC content are either accompanied with higher U/Th, lower Sr/Ba and lower $(La/Yb)_N$, which demonstrates that organic matters are preserved in a deeper, fresh and reduced water environment. Plots of K_2O/Na_2O-SiO_2, SiO_2/Al_2O_3-K_2O/Na_2O, La-Th-Sc, Th-Sc-Zr/10 and Th-Co-Zr/10 indicate a tectonic setting of oceanic island arc or continental island arc.

1. Introduction

Mineralogical, major and trace elemental compositions of clastic rocks are mostly applied to reflect provenance, paleo-climate, paleo-weathering and paleo-tectonic setting. (Nesbitt and Young, 1982; Roser and Korsch, 1986; Condie and Wronkiewicz, 1990; Hayashi et al., 1997; Cullers, 1994; Ghosh and Sarkar, 2010; Zhou et al., 2015). Mineralogical and geochemical compositions are especially useful in reconstructing weathering and sorting history of siltstones, mudstones and shales, as their grain size are too fine and homogeneous to reflect such information. Major oxides of sediments are correlated to their provenance but not entirely in accordance with their source rocks due to compositional fractionation caused by variable weathering under different tectonic settings (McLennan, 1989). Al_2O_3/TiO_2 ratios and Al/Ti ratios retain the values of their parent rocks, whereas Na, K, Ca, Mg, Fe and Mn can be partly or entirely lost during erosion, transport and

* Corresponding author.
E-mail address: liubo@nepu.edu.cn (B. Liu).

https://doi.org/10.1016/j.marpetgeo.2019.09.002
Received 1 February 2019; Received in revised form 30 August 2019; Accepted 1 September 2019
Available online 09 September 2019
0264-8172/

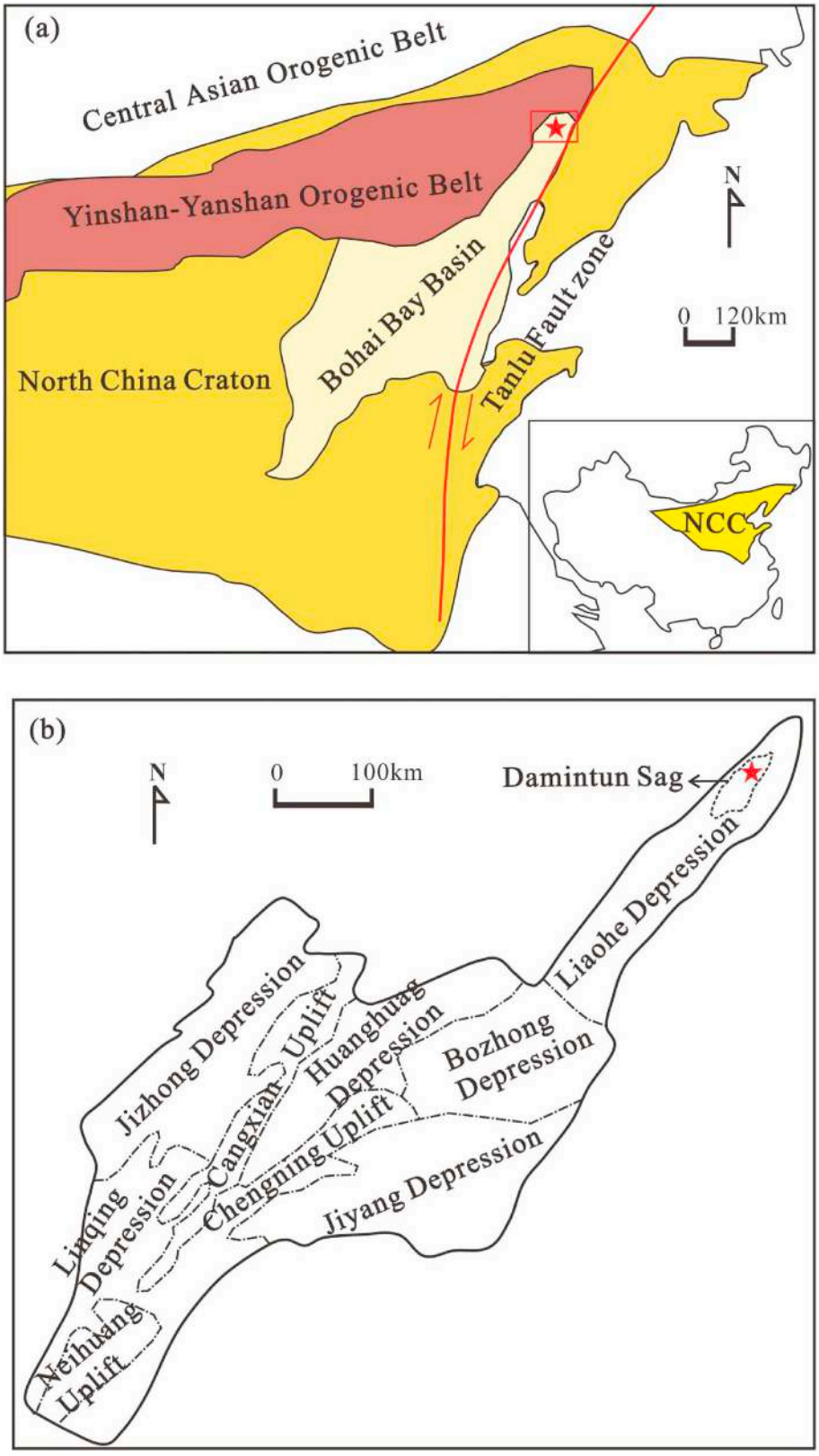

Fig. 1. (a) Geology map of the NCC. (b) Structural map of the Bohai Bay Basin and the location of research target.

sedimentation (Roser and Korsch, 1986; Hayashi et al., 1997). Thus, major oxides are primarily employed to decipher the weathering process of detritus, to comprehend paleo-climate and to reconstruct tectonic setting (Ghosh and Sarkar, 2010).

Immobile trace elements and REEs are resistant to chemical weathering, so they are less leached compared to major oxides during sediments denudation and weathering (Cullers, 1994). Elemental ratios of Cr/Th, La/Th, Co/Th, La/Sc and Th/Sc are widely used to imply provenance of sedimentary rocks (Condie and Wronkiewicz, 1990; Cox et al., 1995; Cullers, 1994). Therefore, trace elements and REEs are

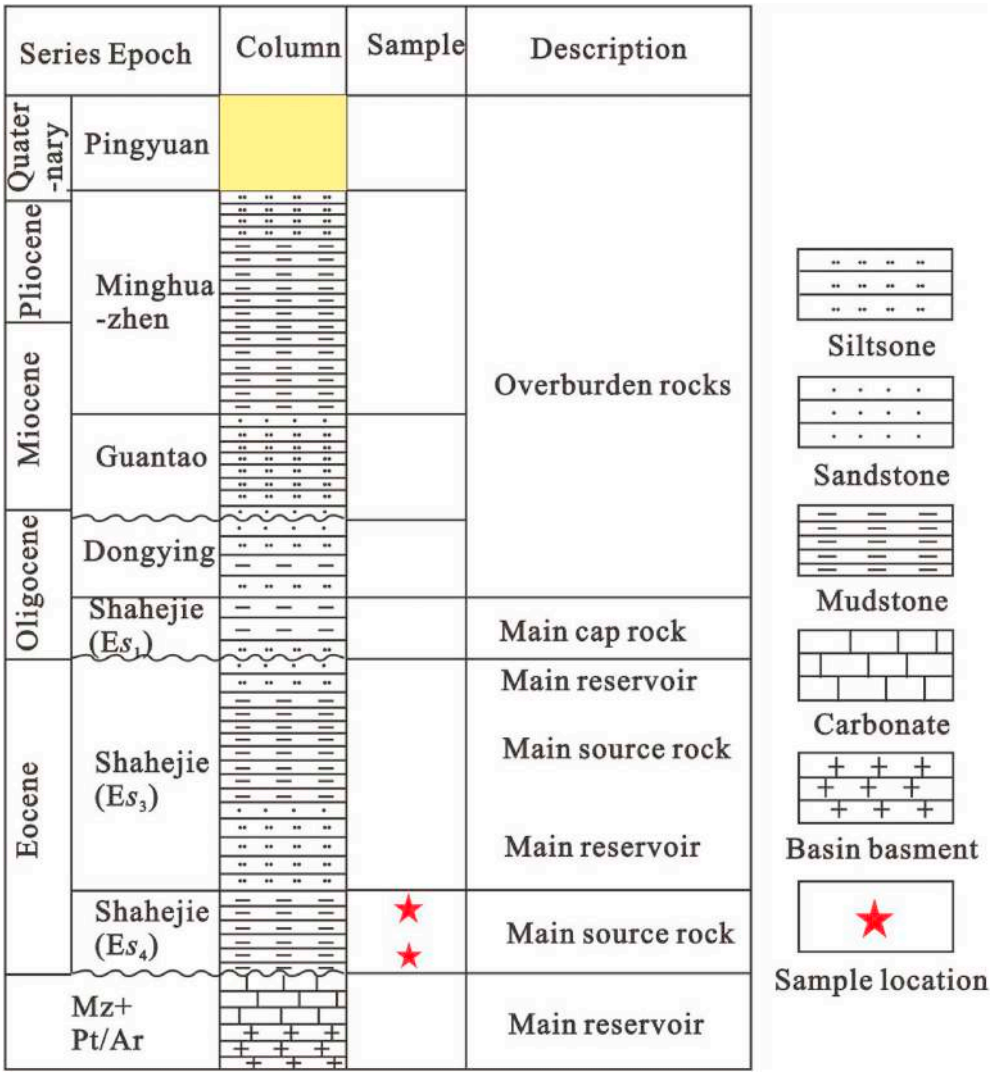

Fig. 2. Stratigraphic column of the Damintun Sag (modified according to Huang et al., 2003).

extensively analyzed to discriminate detritus provenance and tectonic background (Cullers, 1994; Ghosh and Sarkar, 2010; Zhou et al., 2015). With increasing exploration of shale oils & gas in recent years, trace elemental compositions of shales gain more and more attentions in reconstructing paleo-environment which is important for organic matters accumulation (Tao et al., 2016; Zhang et al., 2017; Zhang et al., 2018).

Geochemical compositions and parental rocks of clastic rocks from the Paleogene (exactly the fourth member and the third member of the Shahejie Formation, abbreviated by Es_4 and Es_3 respectively) were analyzed in the southern area of the Bohai Bay Basin. Black shales, one of most significant source rocks contributing for hydrocarbon generation in the Bohai Bay Basin, develop widely in the series of clastic strata from the Es_4 to the Es_3. The Damintun Sag where the Es_4 shale widely distributed and thickly developed is a major target for oil and gas exploration, and locates at the northeast of the Bohai Bay Basin. Previous studies about the Es_4 shales in the Damintun Sag are mainly focused on its potential for hydrocarbon generation (Huang et al., 2003). However, investigations about the provenance, paleo-environment and tectonic setting for these organic rich shales are in great deficiency. Therefore, samples were collected to study the provenance, evaluate the weathering degree of source materials and discriminate the tectonic setting of the Es_4 shales at the Damintun Sag. The aim is to better decipher the provenance, climate and tectonic background for the formation of the Es_4 shales in the Bohai Bay Basin during the Eocene. This may provide valuable insights for exploration of shale oil and gas in this area.

2. Geology background

The Bohai Bay Basin is divided into the Linqing Depression, Jiyang Depression, Huanghua Depression, Jizhong Depression, Bozhong Depression and Liaohe Depression from south to north (Fig. 1). The Damintun Sag is a sub-depression in the Liaohe Depression which has undergone multi-episodic rifting filling and post-rifting filling during the Cenozoic.

Fig. 2 presents the strata column developed in the Damintun Sag. The basement of the sag is mainly composed of the Precambrian metamorphic rocks and magmatic rocks, the middle-upper Proterozoic dolomite, mudstones and sandstones, and some Paleozoic-Mesozoic dolomite and mudstones (Huang et al., 2003). The sag has commenced lacustrine sedimentary rocks since the Eocene. The Eocene-Oligocene is composed of the Shahejie Formation (E*s*) and the Dongying Formation (E*d*). The E*s*, mainly comprised of sandstones and shales with a thickness of 2000–4000 m, is divided into four members (Es_4, Es_3, Es_2, and Es_1, moving upwards) (Huang et al., 2003). The Es_4 and Es_3 shales are the most important hydrocarbon source rocks in the Damintun Sag. The Miocene-Pliocene, comprised of the Guantao Formation (N*g*) and the Minghuazhen Formation (N*m*), is mainly developed with conglomerates

Table 1
Mineral compositions (wt%) and clay mineral compositions (wt%) of the Es_4 shales.

S.N.	Depth (m)	Mineral compositions							clay mineral compositions				
		Clay	Quartz	Plagioclase	Calcite	Siderite	Pyrite	Dolomite	Ilite	Kaolinite	Chlorite	I-S mixed layer	I/S
Upper section of the Es_4 shales													
4	3169.70	41.2	31.3	0.0	0.0	8.8	3.6	15.1	12.0	2.0	3.0	83.0	19
10	3171.06	33.6	28.5	4.8	0.0	2.5	12.6	18.0	11.0	g	5.0	76.0	20
18	3172.74	33.2	49.5	5.2	0.0	5.1	4.3	2.7	11.0	7.0	6.0	76.0	23
36	3177.16	43.5	27.2	3.9	1.6	6.0	2.0	15.8	12.0	5.0	3.0	80.0	23
44	3178.78	38.8	26.3	3.1	2.3	8.7	4.5	16.3	14.0	3.0	2.0	81.0	21
83	3191.13	49.7	40.5	0.0	2.4	4.5	2.9	0.0	13.0	12.0	8.0	67.0	24
91	3192.99	44.7	33.8	0.0	3.0	5.5	5.1	7.9	18.0	3.0	3.0	76.0	21
99	3194.83	37.3	46.6	4.5	1.3	6.3	4.0	0.0	16.0	8.0	7.0	69.0	22
107	3196.86	42.6	25.8	0.0	4.2	4.4	8.4	14.6	16.0	5.0	3.0	76.0	17
Lower section of the Es_4 shales													
288	3285.26	30.0	29.3	13.1	0.0	0.0	2.4	25.2	28.0	4.0	8.0	60.0	12
295	3286.80	47.5	29.8	10.1	0.0	0.0	0.0	12.6	18.0	1.0	2.0	79.0	15
303	3288.77	27.6	37.8	14.2	2.3	2.8	4.7	10.6	16.0	5.0	11.0	68.0	12
311	3290.89	31.3	38.0	17.5	0.0	2.2	3.6	7.4	15.0	3.0	10.0	72.0	19
334	3296.12	40.5	29.7	6.6	2.7	1.6	0.0	18.9	18.0	1.0	2.0	79.0	13
342	3297.97	40.0	30.6	8.2	1.6	0.0	2.5	17.1	15.0	1.0	5.0	79.0	17
350	3299.71	30.4	50.2	8.8	3.4	0.0	5.6	1.6	12.0	3.0	7.0	78.0	20
358	3301.41	40.5	40.5	6.6	0.0	2.5	8.0	1.9	16.0	3.0	3.0	78.0	21
366	3303.37	41.8	31.2	6.3	0.0	0.0	2.6	18.1	19.0	0.0	1.0	80.0	16
374	3305.42	41.8	39.7	5.0	0.0	9.7	1.7	2.1	15.0	2.0	5.0	78.0	24
382	3307.29	33.0	28.5	5.7	1.8	3.7	5.9	21.4	13.0	2.0	7.0	78.0	20
383	3307.51	43.5	31.2	9.2	3.6	1.4	2.3	8.8	*	*	*	*	*
390	3308.99	33.5	37.3	12.9	9.4	0.0	4.8	2.1	19.0	5.0	6.0	70.0	17
406	3312.82	35.2	26.7	10.4	6.2	0.0	2.0	19.5	17.0	3.0	5.0	75.0	18
436	3329.78	41.4	36.3	5.2	7.5	0.0	5.3	4.3	14.0	5.0	5.0	76.0	21
444	3331.92	37.5	44.8	5.7	2.5	0.0	2.8	6.7	12.0	5.0	8.0	75.0	18
449	3333.52	32.7	47.4	6.8	5.2	0.8	3.6	3.5	8.0	9.0	14.0	69.0	16

S.N. represents sample number. * means not analyzed.

Table 2
Major element compositions (wt%) of the E_{s4} shales.

Sample number	Depth (m)	SiO_2	Al_2O_3	Fe_2O_3	CaO	MgO	K_2O	BaO	Cr_2O_3	MnO	Na_2O	P_2O_5	SrO	TiO_2	LOI	Total	K_2O/Al_2O_3	ICV	CIA	PIA
Upper section of the Es_4 shales																				
4	3169.7	47.30	15.05	7.98	5.16	4.78	2.16	0.05	0.02	0.13	0.57	0.31	0.03	0.86	15.35	99.75	0.14	0.74	59.71	64.23
10	3171.1	52.60	14.40	9.77	0.78	3.18	1.16	0.05	0.02	0.10	0.57	0.21	0.02	0.94	16.10	99.90	0.08	0.28	82.34	92.89
18	3172.7	37.50	14.00	20.40	1.37	4.09	1.05	0.06	0.01	0.38	0.51	0.22	0.02	0.79	19.00	99.40	0.08	1.43	75.54	82.33
23	3174.0	52.20	16.45	8.82	1.10	2.93	1.48	0.06	0.02	0.13	0.59	0.18	0.02	0.94	14.80	99.72	0.09	0.97	74.20	82.17
28	3175.4	51.20	16.45	7.93	1.30	2.48	1.48	0.08	0.02	0.06	0.65	0.21	0.02	1.09	16.50	99.47	0.09	0.91	72.68	79.95
36	3177.2	41.30	14.05	8.75	7.21	5.81	1.85	0.06	0.02	0.14	0.50	0.41	0.03	0.88	18.65	99.66	0.13	1.17	55.26	57.21
44	3178.8	41.30	13.75	9.81	6.00	5.83	1.56	0.06	0.01	0.16	0.49	0.29	0.03	0.90	19.65	99.84	0.11	1.80	48.45	48.06
72	3188.1	58.50	13.65	4.54	2.26	1.42	1.18	0.12	0.02	0.02	0.59	0.18	0.02	0.89	16.15	99.54	0.09	0.20	81.21	92.19
83	3191.1	51.00	13.20	8.59	4.29	2.32	1.11	0.05	0.01	0.15	0.51	0.23	0.02	0.75	17.65	99.88	0.08	0.84	61.50	64.23
91	3193.0	41.00	14.55	11.20	6.33	3.77	1.49	0.06	0.02	0.20	0.51	0.59	0.03	1.10	19.15	100.00	0.10	0.80	59.55	62.34
99	3194.8	53.10	13.40	9.40	2.12	1.69	0.91	0.07	0.01	0.18	0.51	0.24	0.01	0.83	17.80	100.27	0.07	0.57	72.58	77.63
107	3196.9	40.40	14.00	8.82	6.92	3.40	1.34	0.07	0.02	0.19	0.44	0.80	0.03	0.94	22.40	99.77	0.10	0.50	65.17	69.74
Lower section of the Es_4 shales																				
288	3285.3	39.50	10.05	7.72	10.35	5.87	1.52	0.07	0.01	0.19	1.27	0.30	0.05	0.64	22.30	99.84	0.15	1.65	37.46	34.13
295	3286.8	49.30	15.50	6.33	4.54	4.53	3.22	0.04	0.02	0.09	0.89	0.25	0.03	0.98	14.50	100.22	0.21	1.12	55.93	60.42
303	3288.8	49.30	11.05	9.34	4.40	3.96	1.24	0.03	0.01	0.21	1.36	0.17	0.02	0.67	18.40	100.16	0.11	0.78	60.33	63.79
311	3290.9	51.80	12.25	8.05	5.78	3.49	1.34	0.04	0.02	0.10	1.28	0.27	0.04	0.90	14.35	99.71	0.11	1.02	48.39	47.99
334	3296.1	51.70	13.70	6.68	4.90	4.21	2.19	0.04	0.02	0.13	0.89	0.16	0.04	0.91	14.45	100.02	0.16	0.98	67.96	80.09
342	3298.0	50.90	15.50	6.29	4.70	3.21	2.17	0.08	0.02	0.10	1.09	0.26	0.04	1.07	13.80	99.23	0.14	0.56	65.94	74.24
350	3299.7	62.60	12.80	6.56	1.10	1.73	1.43	0.05	0.01	0.11	0.90	0.14	0.03	0.75	11.70	99.91	0.11	0.37	75.59	87.27
358	3301.4	55.40	17.20	6.79	1.14	2.14	2.22	0.05	0.02	0.05	0.96	0.30	0.04	1.13	12.55	99.99	0.13	0.42	70.36	80.70
366	3303.4	55.30	18.35	5.17	1.83	2.86	2.96	0.07	0.02	0.03	0.92	0.16	0.05	1.23	10.70	99.65	0.16	0.35	72.38	89.47
374	3305.4	49.20	13.45	13.25	1.73	3.90	1.59	0.06	0.02	0.22	0.74	0.18	0.04	0.93	13.95	99.26	0.12	1.39	66.63	73.50
382	3307.3	38.30	12.20	10.75	8.60	5.44	1.61	0.04	0.02	0.30	0.70	0.20	0.05	0.83	20.40	99.44	0.13	0.89	50.34	50.45
383	3307.5	44.60	12.20	8.53	8.22	4.24	1.63	0.04	0.02	0.19	0.82	0.25	0.05	0.84	17.65	99.28	0.13	1.31	47.97	47.34
390	3309.0	55.90	11.10	4.85	6.22	1.70	1.38	0.06	0.01	0.05	0.96	0.25	0.04	0.59	16.40	99.51	0.12	0.46	67.69	75.72
406	3312.8	40.80	11.55	6.46	11.85	4.44	1.47	0.08	0.01	0.14	0.86	0.23	0.07	0.73	21.70	100.39	0.13	1.19	45.21	43.91
436	3329.8	53.70	16.55	6.77	4.41	2.47	2.31	0.10	0.02	0.07	0.89	0.32	0.05	1.02	11.60	100.28	0.14	0.38	74.22	89.34
444	3331.9	52.70	14.80	7.68	4.45	2.90	1.93	0.04	0.02	0.11	0.86	0.50	0.05	1.10	12.35	99.49	0.13	0.73	63.00	68.70
449	3333.5	48.20	15.70	9.85	5.23	3.23	1.35	0.08	0.02	0.09	0.71	0.34	0.05	1.23	13.65	99.73	0.09	0.72	69.40	74.91

Table 3
Trace elements, trace elemental ratios, TOC and Ti concentrations (ppm) in the Es4 shales, intermediate rocks, felsic rocks and mafic rocks collected from the northeast of the North China Craton.

Sample number	Depth (m)	Ti	Sc	V	Cr	Co	Ni	Ga	Y	Zr	Nb	Hf	Ta	Th	U	Rb	Sr	Cs	Ba	Pb	U/Th	V/Cr	V/(V + Ni)	Ni/Co	Sr/Ba	TOC
Upper section of the Es_4 shales																										
4	3169.7	5160	15	113	107	18	67	20	15	80	16	2.2	1.1	7.6	1.1	68	275	5.5	500	13	0.1	1.1	0.5	3.7	0.6	1.6
10	3171.1	5640	18	151	122	27	118	20	16	97	18	2.4	1.1	8.1	1.5	55	150	5.1	430	17	0.2	1.2	0.6	4.4	0.3	7.5
18	3172.7	4740	20	139	106	26	89	19	23	111	15	2.5	1.0	7.3	1.4	51	159	4.6	480	25	0.2	1.3	0.6	3.4	0.3	
23	3174.0	5640	17	169	123	31	121	23	19	99	18	2.6	1.1	7.8	1.5	67	177	5.7	540	21	0.2	1.4	0.6	3.9	0.3	
28	3175.4	6540	17	151	140	45	156	23	19	109	23	2.9	1.3	9.4	2.0	72	183	6.2	690	25	0.2	1.1	0.5	3.4	0.3	
36	3177.2	5280	14	105	108	18	51	18	17	109	17	2.7	1.0	7.4	1.1	67	298	5.4	510	9	0.1	1.0	0.5	2.9	0.6	
44	3178.8	5400	13	100	105	38	92	17	15	96	16	2.5	1.0	8.1	1.4	63	250	4.8	480	10	0.2	1.0	0.5	2.4	0.5	3.3
72	3188.1	5340	16	146	121	23	92	20	15	90	17	2.4	1.0	8.2	1.8	59	181	5.4	870	21	0.2	1.2	0.5	4.0	0.2	
83	3191.1	4500	15	147	101	18	80	18	18	84	14	2.1	0.9	7.0	1.5	53	224	4.5	450	11	0.2	1.5	0.6	4.4	0.5	7.1
91	3193.0	6600	15	122	120	22	73	18	18	103	20	2.5	1.2	7.4	1.2	65	318	5.3	510	11	0.2	1.0	0.5	3.4	0.6	
99	3194.8	4980	15	145	107	20	87	19	19	89	15	2.2	1.0	7.6	1.6	52	193	4.6	600	14	0.2	1.4	0.6	4.3	0.3	6.2
107	3196.9	5640	14	128	123	21	77	19	18	104	18	2.3	1.1	7.6	1.3	64	301	4.9	590	13	0.2	1.0	0.5	3.6	0.5	
Lower section of the Es_4 shales																										
288	3285.3	3840	11	74	92	13	45	15	11	61	12	1.5	0.7	5.0	0.8	52	471	3.7	670	14	0.2	0.8	0.4	3.4	0.7	6.2
295	3286.8	5880	17	122	127	28	83	23	15	91	17	2.4	1.1	7.2	0.9	90	352	5.5	340	11	0.1	1.0	0.5	3.0	1.0	
303	3288.8	4020	12	100	96	22	80	15	11	55	12	1.4	0.8	5.2	0.9	45	256	2.9	340	13	0.2	1.0	0.5	3.6	0.8	6.3
311	3290.9	5400	14	112	119	23	80	17	16	77	15	1.9	1.0	6.2	1.3	54	382	3.4	410	15	0.2	0.9	0.5	3.4	0.9	5.9
334	3296.1	5460	15	103	119	24	66	19	15	85	15	2.1	0.9	7.3	1.3	73	413	4.6	350	13	0.2	0.9	0.5	2.8	1.2	4.0
342	3298.0	6420	18	139	149	26	70	24	18	87	21	2.2	1.2	8.2	1.4	81	474	5.7	720	17	0.2	0.9	0.5	2.7	0.7	4.8
350	3299.7	4500	14	119	112	22	87	19	10	68	13	1.7	0.9	6.8	1.2	63	300	4.4	460	12	0.2	1.1	0.5	4.0	0.7	
358	3301.4	6780	19	145	147	33	146	26	22	93	20	2.4	1.2	9.2	2.3	96	387	6.2	470	20	0.3	1.0	0.5	4.4	0.8	
366	3303.4	7380	19	156	157	33	117	27	12	98	19	2.7	1.3	8.7	1.6	94	441	6.4	640	19	0.2	1.0	0.5	3.6	0.7	
374	3305.4	5580	15	111	116	18	77	19	14	75	15	1.8	0.9	6.8	0.8	65	335	4.1	540	14	0.1	1.0	0.5	4.2	0.6	4.0
382	3307.3	4980	13	93	106	14	51	19	14	67	14	1.7	0.9	6.2	0.8	63	526	3.9	320	10	0.1	0.9	0.5	3.7	1.6	
383	3307.5	5040	13	98	109	17	56	18	15	75	15	1.9	0.9	6.9	1.0	67	531	4.1	390	11	0.1	0.9	0.5	3.3	1.4	5.8
390	3309.0	3540	11	87	89	16	53	16	10	54	11	1.4	0.7	6.1	0.9	65	436	4.4	580	12	0.1	1.0	0.5	3.3	0.8	5.3
406	3312.8	4380	11	87	96	11	39	16	11	62	13	1.7	0.9	6.3	0.8	70	631	4.0	720	13	0.1	0.9	0.5	3.5	0.9	2.6
436	3329.8	6120	16	120	135	23	92	24	13	74	17	2.0	1.1	9.0	1.0	96	508	6.2	880	22	0.1	0.9	0.5	4.0	0.6	
444	3331.9	6600	18	125	132	24	93	21	31	94	18	2.5	1.2	7.7	1.1	80	482	5.2	350	14	0.1	0.9	0.5	3.8	1.4	3.0
449	3333.5	7380	19	131	156	31	100	24	20	83	21	2.1	1.2	8.3	1.0	67	503	4.6	670	18	0.1	0.8	0.5	3.3	0.8	
Intermediate-1, Mesozoic, Sun et al., 2017																										
		2760	*	61	*	8	7	18	14	130	7	3.2	0.4	7.3	1.5	102	317	*	*	21	0.2	*	*	0.8	*	*
Intermediate-2, Mesozoic, Yang and Li, 2008																										
		3480	8	*	156	*	82	*	13	164	6	3.9	0.4	11.2	2.8	113	461	*	719	18	0.2			*	*	*
Felsic-1, Mesozoic, Sun et al., 2017																										
		1140		2		0	1	20	13	215	14	5.1	0.7	12.5	1.3	130	76	*	601	18	0.1	*	*	3.7	*	*
Felsic-2, Mesozoic, Yang and Li, 2008																										
		2820	4	*	0	*	1	*	28	283	12	6.5	0.5	4.9	0.7	105	415	*	1246	16	0.2	*	*	*	*	*
Mafic-1, Cenozoic, Li et al., 2014																										
		11340	24	*	368	50	204	*	17	144	32	2.5	1.5	1.8	0.5	20	841	*	343	*	0.3	*	*	4.1	*	*
Mafic-2, Mesozoic, Yang and Li, 2008																										
		6540	17	*	2	*	5	*	21	163	9	3.9	0.5	2.0	0.4	35	658	*	621	6	0.2	*	*	*	*	*

* not analyzed in these references.

Table 4
Rare earth element concentrations (ppm) in the Es_4 shales, intermediate rocks, felsic rocks and mafic rocks collected from the northeast of the North China Craton.

Sample number	Depth (m)	La	Ce	Pr	Nd	Sm	Eu	Gd	Tb	Dy	Y	Ho	Er	Tm	Yb	Lu	$(La/Yb)_N$	Eu_N/Eu^*	$(Gd/Yb)_N$	Eu_{SN}/Eu^*
Upper section of the Es_4 shales																				
4	3169.7	34.80	67.30	7.58	28.00	5.21	1.28	4.31	0.64	3.53	19.80	0.75	2.01	0.27	1.83	0.28	13.19	0.29	1.95	1.42
10	3171.1	34.50	68.90	7.91	29.50	5.90	1.58	5.15	0.76	3.95	20.30	0.78	2.12	0.29	1.92	0.27	12.46	0.31	2.22	1.52
18	3172.7	35.30	70.40	7.98	30.60	5.91	1.42	5.23	0.79	4.41	25.10	0.87	2.35	0.33	2.15	0.31	11.39	0.27	2.01	1.35
23	3174.0	36.20	67.20	7.95	28.50	5.33	1.32	4.75	0.72	4.07	21.80	0.78	2.08	0.28	1.95	0.29	12.88	0.28	2.02	1.38
28	3175.4	43.10	81.30	9.22	33.90	6.54	1.63	5.28	0.78	4.25	23.20	0.86	2.30	0.33	2.10	0.32	14.24	0.29	2.08	1.45
36	3177.2	33.00	62.20	7.16	26.30	4.87	1.31	4.24	0.66	3.45	19.80	0.67	1.74	0.26	1.62	0.24	14.13	0.31	2.17	1.50
44	3178.8	33.90	62.50	7.16	25.40	4.87	1.22	3.92	0.60	3.13	18.20	0.62	1.77	0.22	1.67	0.25	14.08	0.29	1.94	1.44
72	3188.1	34.30	67.70	7.82	28.90	5.17	1.10	4.23	0.61	3.64	18.70	0.73	1.94	0.29	1.84	0.28	12.93	0.25	1.90	1.24
83	3191.1	35.60	68.90	7.66	29.10	5.79	1.31	4.62	0.71	3.98	22.10	0.82	2.29	0.30	1.99	0.28	12.41	0.27	1.92	1.30
91	3193.0	34.80	65.30	7.39	27.00	5.43	1.35	4.48	0.64	3.56	20.60	0.71	1.90	0.28	1.88	0.25	12.84	0.29	1.97	1.45
99	3194.8	35.00	69.40	7.89	29.50	5.76	1.37	4.87	0.68	4.05	21.50	0.77	1.95	0.31	1.80	0.28	13.49	0.27	2.24	1.39
107	3196.9	36.60	69.70	7.93	29.60	5.95	1.36	4.36	0.66	3.81	21.00	0.75	1.90	0.27	1.83	0.26	13.87	0.28	1.97	1.36
Lower section of the Es_4 shales																				
288	3285.3	20.90	40.60	4.71	18.20	3.24	0.75	2.66	0.41	2.61	12.80	0.47	1.32	0.17	1.32	0.15	10.98	0.27	1.67	1.32
295	3286.8	32.60	63.20	7.37	28.00	5.43	1.10	4.49	0.64	4.02	18.40	0.73	2.08	0.31	1.84	0.25	12.29	0.24	2.02	1.18
303	3288.8	23.20	46.20	5.29	19.90	4.05	0.88	3.14	0.51	3.13	14.60	0.53	1.52	0.24	1.38	0.18	11.66	0.26	1.88	1.24
311	3290.9	28.10	57.60	6.67	27.10	5.48	1.32	4.88	0.68	4.06	19.20	0.78	1.95	0.28	1.58	0.23	12.34	0.27	2.56	1.38
334	3296.1	29.70	58.50	6.87	27.20	5.20	1.14	4.38	0.66	3.66	17.80	0.70	2.01	0.25	1.65	0.25	12.49	0.25	2.20	1.25
342	3298.0	34.80	69.80	8.47	34.50	7.36	1.61	6.15	0.91	4.66	21.50	0.82	2.31	0.27	1.92	0.26	12.57	0.25	2.65	1.26
350	3299.7	26.80	51.20	5.86	21.90	4.25	0.72	3.13	0.45	2.68	14.00	0.52	1.49	0.21	1.55	0.19	11.99	0.21	1.67	1.02
358	3301.4	40.40	80.80	9.48	37.10	7.87	1.80	6.94	0.97	5.72	25.80	0.96	2.76	0.36	2.42	0.32	11.58	0.26	2.37	1.32
366	3303.4	34.10	66.30	7.72	29.20	5.59	1.15	4.27	0.66	3.86	17.80	0.72	1.94	0.29	1.93	0.24	12.26	0.25	1.83	1.20
374	3305.4	29.20	56.80	6.52	24.60	5.01	1.21	4.29	0.62	3.77	18.60	0.69	1.93	0.29	1.76	0.25	11.51	0.28	2.02	1.39
382	3307.3	27.10	52.80	5.86	22.70	4.41	0.98	3.86	0.56	3.25	16.50	0.61	1.82	0.25	1.63	0.21	11.53	0.25	1.96	1.27
383	3307.5	28.80	58.00	6.64	26.60	5.11	1.22	4.28	0.61	3.66	17.20	0.67	1.76	0.25	1.64	0.20	12.18	0.28	2.16	1.39
390	3309.0	22.40	41.60	4.75	17.50	3.37	0.80	2.70	0.44	2.49	13.10	0.46	1.41	0.19	1.34	0.18	11.59	0.28	1.67	1.34
406	3312.8	23.80	46.20	5.29	20.30	3.64	0.76	3.02	0.45	2.79	13.10	0.48	1.50	0.19	1.29	0.17	12.80	0.24	1.94	1.20
436	3329.8	32.80	60.80	6.63	24.00	4.56	0.94	3.69	0.54	3.32	16.60	0.63	1.94	0.27	1.95	0.24	11.67	0.24	1.57	1.20
444	3331.9	41.30	92.50	12.00	51.70	12.20	2.77	10.30	1.41	7.48	32.80	1.21	3.20	0.36	2.24	0.31	12.79	0.26	3.80	1.33
449	3333.5	35.20	68.10	7.87	30.00	6.13	1.56	5.23	0.77	4.48	22.60	0.85	2.30	0.35	2.22	0.28	11.00	0.29	1.95	1.46
Intermediate-1, Mesozoic, Sun et al., 2017																				
		32.00	63.00	7.11	26.60	4.26	1.05	3.19	0.46	2.44	14.48	0.48	1.35	0.21	1.33	0.21	16.69	0.30	1.98	1.48
Intermediate-2, Mesozoic, Wang and Cheng, 2012																				
		26.20	49.50	5.73	20.50	3.82	1.02	3.26	0.42	2.12	12.70	0.42	1.01	0.15	0.97	0.14	18.73	0.31	2.78	1.59
Felsic-1, Mesozoic, Sun et al., 2017																				
		90.00	167.00	16.35	52.00	6.32	1.05	4.16	0.57	2.57	12.72	0.48	1.32	0.17	1.03	0.15	60.61	0.21	3.34	1.05
Felsic-2, Mesozoic, Yang and Li, 2008																				
		26.20	49.50	5.73	20.50	3.82	1.02	3.26	0.42	2.12	12.70	0.42	1.01	0.15	0.97	0.14	10.87	0.28	1.73	1.41
Mafic-1, Cenozoic, Li et al., 2014																				
		18.90	37.00	4.81	19.10	4.26	1.40	4.20	0.62	3.45	17.20	0.64	1.63	0.23	1.39	0.20	9.43	0.36	2.50	1.79
Mafic-2, Mesozoic, Yang and Li, 2008																				
		23.20	51.60	6.65	28.00	5.40	1.59	4.94	0.75	4.19	20.90	0.80	2.13	0.33	2.04	0.32	7.89	0.33	2.00	1.63

and sandstones.

3. Sample collection and analysis

Twenty-nine core samples were obtained from the Es_4 black shales in S352 well whose location is marked by the pentacle in Fig. 1. Twelve samples are collected from the depth of 3169–3197 m, and the other seventeen samples are collected from the depth of 3285–3334 m. Shales from the depth of 3198–3284 m are not analyzed in this research due to high contents of calcite and dolomite. All the 29 Es_4 shales were analyzed for composition of bulk mineralogy, major oxides and trace elements including REEs.

Firstly, shale samples were crushed to powders with grain size around 10 μm by the Retsch Vibratory Disc Mill RS 200. Then, the rock powders were put in the fillister on the sample table of the Rigaku D/Max-2500 X-ray diffraction spectrometer. Powder samples were continuously rotated and scanned from 5 to 80 °C with $\lambda = 1.54$ Å, V = 40kv, I = 200 mA, sampling step width of 0.02°, per step of 0.5s. Mineralogical compositions are given in Table 1.

Secondly, 4 g rock powders with grain size around 300 meshes were pressed to a disk with diameter of 32 mm under a pressure of 32 MPa. Then this disk was analyzed with an Axios 4.0 X-ray fluorescence spectrometer. Operation condition for the XRF machine was V = 60 kV, I = 120 mA and P = 4 kW. For major oxides measurement, the average precision is controlled to be less than 2%. Results of major oxides are given in Table 2.

For the measurement of trace elements including REEs, shale powders with grain size around 200 meshes were digested with a HCl-HF-HNO_3 mixture at 190 °C until the solution was evaporated to dryness. This evaporated sample was digested again with 5 ml mixture of 1HCl:3HNO_3 for 10min and then diluted by 95 ml distill water. The solution was analyzed with a Perkin-Elmer SCIEX Model ELAN DRC II Inductively Coupled Plasma-Mass Spectrometer. Details of the analytical procedure are given by Balaram and Rao (2003), and analytical precision is better than 5%. TOC contents are measured on the Rock-Eval II instrument at the Changjiang University following the procedure given by Espitalié et al. (1985). Analytical results for trace elements and TOC are presented in Table 3 and Table 4.

4. Results

4.1. Mineralogy

The mineralogical compositions of the Es_4 shales are shown in Table 1. Predominant minerals of the Es_4 shales are clay minerals and quartz. Clay minerals range from 27.6% to 49.7% with an average of 38.2%, and quartz lies between 25.8% and 50.2% with an average of 35.3%. Clay minerals are consisted of illite, kaolinite, chlorite and Illite-

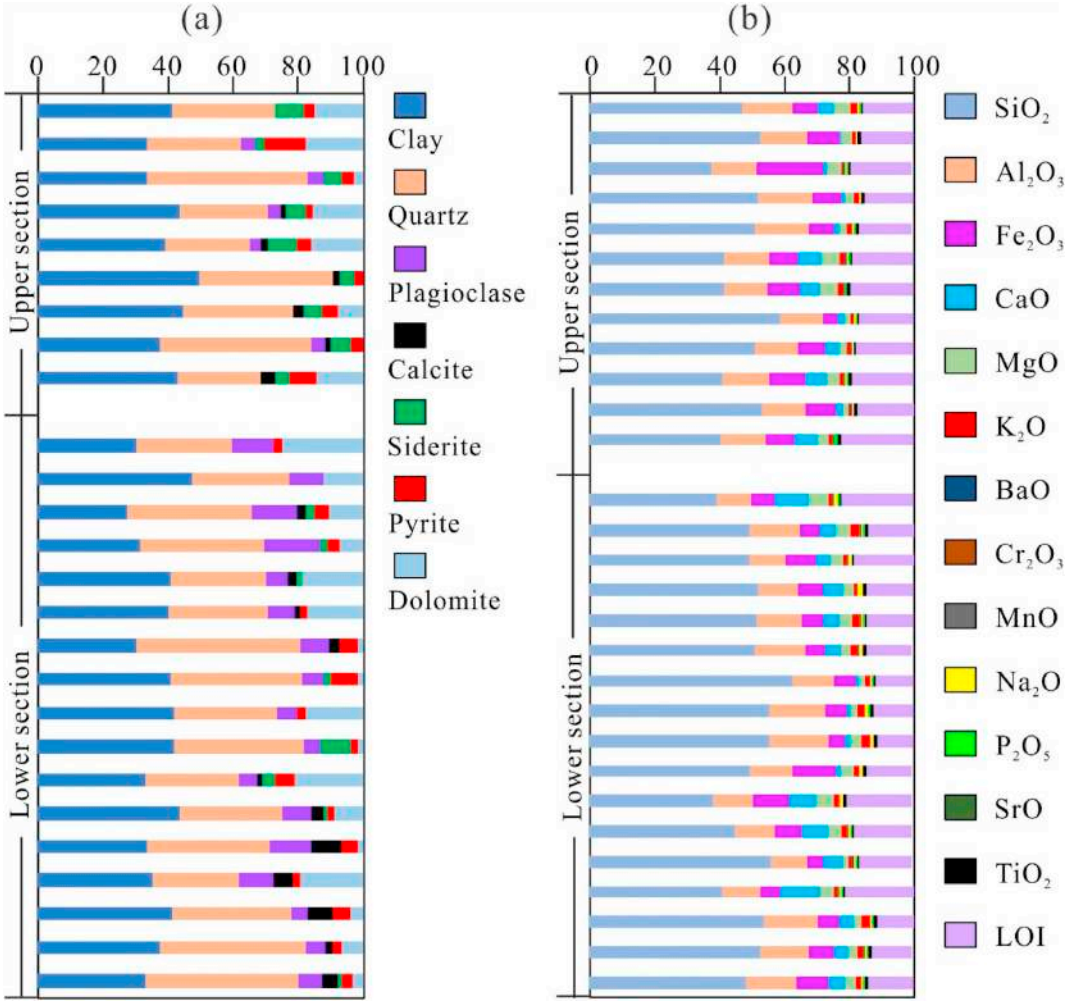

Fig. 3. Vertical variations of mineral compositions and major elemental compositions of the Es_4 shales.

Smectite mixed-layer, among which Illite-Smectite mixed-layer is dominant. Carbonate minerals are comprised of calcite (1.3% ~ 9.4%, average of 3.6%), siderite (0.8% ~ 9.7%, average of 4.5%) and dolomite (1.6% ~ 25.2%, average of 11.3%). Other minerals are plagioclase (3.1% ~ 17.5%, average of 7.9%) and pyrite (1.7% ~ 12.6%, average of 4.4%). No significant variation of these minerals is observed between the lower and upper sections except for plagioclase which shows a slightly higher content at the lower section with a depth of 3285–3334 m (Fig. 3a and b).

4.2. Major oxides distribution

Major oxides contents of these analyzed shales are shown in Table 2. Most major oxides contents of shales at different depths are located at a relatively narrow extent, except for the SiO_2 that presents a range from 37.5% to 62.6%. Contents of Na_2O and K_2O at the deeper depth (0.70% ~ 1.36% Na_2O, 1.24% ~ 3.22% K_2O) are higher compared to that at the shallower depth (0.44% ~ 0.65% Na_2O, 0.91% ~ 2.16% K_2O), and other major oxides show similar distribution signature between the two sections (Table 2, Fig. 3b).

Fig. 4 shows the plots of major oxides normalized by the PAAS (Post Archean Australian Average Shale) values from Taylor and McLennan (1985). Correlations of Na_2O vs. Al_2O_3, MgO vs. Al_2O_3, SiO_2 vs. Al_2O_3 and Fe_2O_3 vs. Al_2O_3 of these shale samples are not obvious, which probably imply that these major oxides are not only hosted by clay minerals. K_2O concentration is depleted to that of the PAAS and shows a positive relationship with Al_2O_3 and Illite-Smectite mixed layer (Fig. 5a, Fig. 5b), which possibly suggest that the minerals hosting K_2O are mainly Illite-Smectite mixed layer in the Es_4 shales. Na_2O is moderately depleted with respect to the PAAS and decreases with the upward decreased content of plagioclase (Figs. 4 and 5c), which may reflects more transformation of plagioclase to clay minerals in the upper section (Fig. 3b). A positive relationship between CaO and MgO is detected, and moreover their contents are higher in most samples compared to the PAAS (Figs. 4 and 5d). Considering of the slightly higher LOI which is mainly attributed to losses of CO_2 and organic matters (Table 2), enrichment of CaO and MgO in these shales is possibly resulted from carbonate minerals. There are 13 and 16 samples showing depleted MnO and enriched MnO compared to the PAAS, respectively. Fe_2O_3 is mainly hosted in siderite and pyrite, which is confirmed by their positive linear relationship (Fig. 5e). All shales are slightly depleted in SiO_2 and Al_2O_3 compared to the PAAS (Fig. 4). The positive relationship between SiO_2 and quartz implies that SiO_2 is mainly hosted by quartz (Fig. 5f).

4.3. Trace elements and REEs distribution

Trace elemental data are normalized by the UCC (average upper continental crust, Taylor and McLennan, 1985). Fig. 6 gives distribution patterns of trace elements with compatible elements plotted at left and incompatible elements plotted at right. This decreasing compatible order of trace elements is associated with typical igneous differentiation series (Ghosh and Sarkar, 2010). With respect to the UCC, the Es_4 shales are significantly depleted in Sc, but slightly enriched in V, Cr and Co

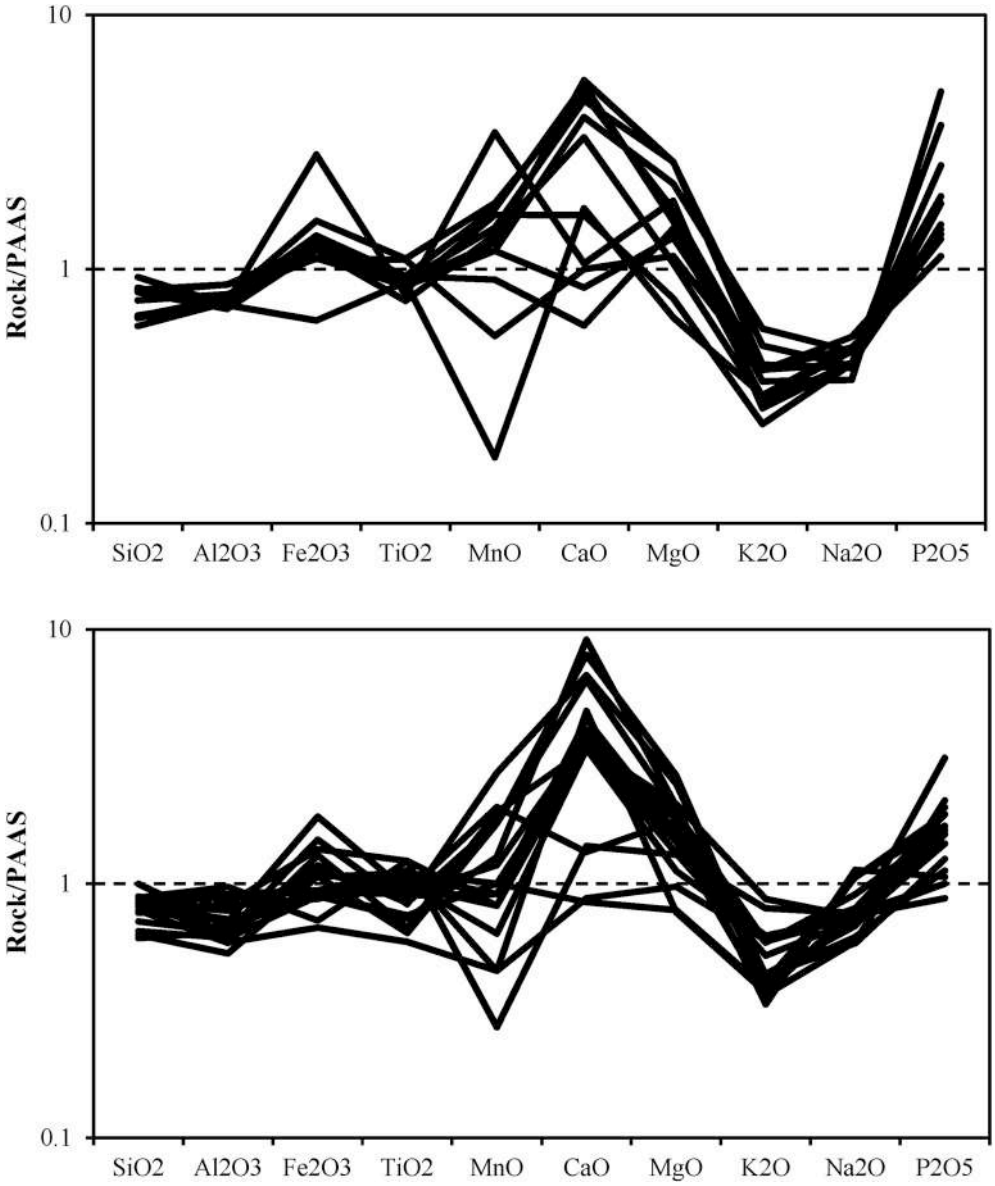

Fig. 4. Distribution pattern of the PAAS normalized major elements of (a) upper section and (b) lower section of the Es_4 shales.

(Fig. 6). With respect to mafic igneous rocks, the Es_4 shales show comparable distribution of Ti, Sc, Cr and Ni. Slight depletions of HFSE (high field-strength elements) such as Zr, Nb, Hf, Ta, Th and U are also observed compared with the UCC, whereas Y contents are close to the UCC (Fig. 6). Concentrations of the Large Ion Lithophile elements (LIL, Sr, Cs, Ba and Pb) are similar to or greater than the UCC. On the other hand, Rb is depleted compared to the UCC. Lower Rb content generally relates to low concentration of K_2O which is mainly hosted by Illite-Smectite mixed-layer.

Table 4 presents the results of REE + Y. Fig. 7 and Fig. 10 show the C1-chondrite normalized and the PAAS normalized REE + Y patterns of the Es_4 shales, respectively. In general, all the Es_4 shales from different depths have similar C1-chondrite normalized and the PAAS normalized REE + Y patterns. REEs contents of the Es_4 shales are enriched compared to that of the C1-chondrite and slightly depleted compared to that of the PAAS. Eu anomalies are expressed by Eu_{SN}/Eu^* (Eu_{SN} represents Eu normalized by the PAAS, and $Eu^* = 0.67Sm_{SN} + 0.33Tb_{SN}$) and Eu_N/Eu^* (Eu_N represents Eu normalized by the C1-chondrite, and $Eu^* = 0.67Sm_N + 0.33Tb_N$). In Table 4, the Es_4 shales show high $(La/Yb)_N$ ratios (10.98–14.24, in average of 12.45), pronounced negative Eu_N/Eu^* (0.21–0.31, with an average value of 0.27) and positive Eu_{SN}/Eu^* (1.02–1.52, with an average value of 1.33). Remarkably, these C1-chondrite normalized REE + Y distributions of the Es_4 shales are very similar to that of mafic-intermediate igneous rocks which composed basin basement of the southern Liaohe Depression (Fig. 7).

4.4. Weathering proxies

Cox et al. (1995) proposed the Index of Compositional Variability, which is expressed by $ICV = [(Fe_2O_3^* + K_2O + Na_2O + CaO^* + MgO^* + MnO + TiO_2)/Al_2O_3]$ (all in weight contents), to indicate weathering degree. All $Fe_2O_3^*$, CaO^* and MgO^* in this research represent corresponding oxides from the silicates rather than carbonate rocks, and are corrected by Fe (pyrite), CO_2 (calcite) and CO_2 (dolomite) according to Fedo et al. (1995) and Zhou et al. (2015). This index reflects the measuring compositional maturity for sediments as alumina accumulating in a compositional mature rock relative to the other major cations. The Es_4 shales show ICV values locating between 0.20 and 1.80 with a mean value of 0.85. ICV in the shallower section (0.20–1.80, average of 0.85) is slightly higher than that in the deeper section (0.35–1.65, average of 0.84) (Table 2).

K_2O/Al_2O_3 ratio is an index for shales composition, which is

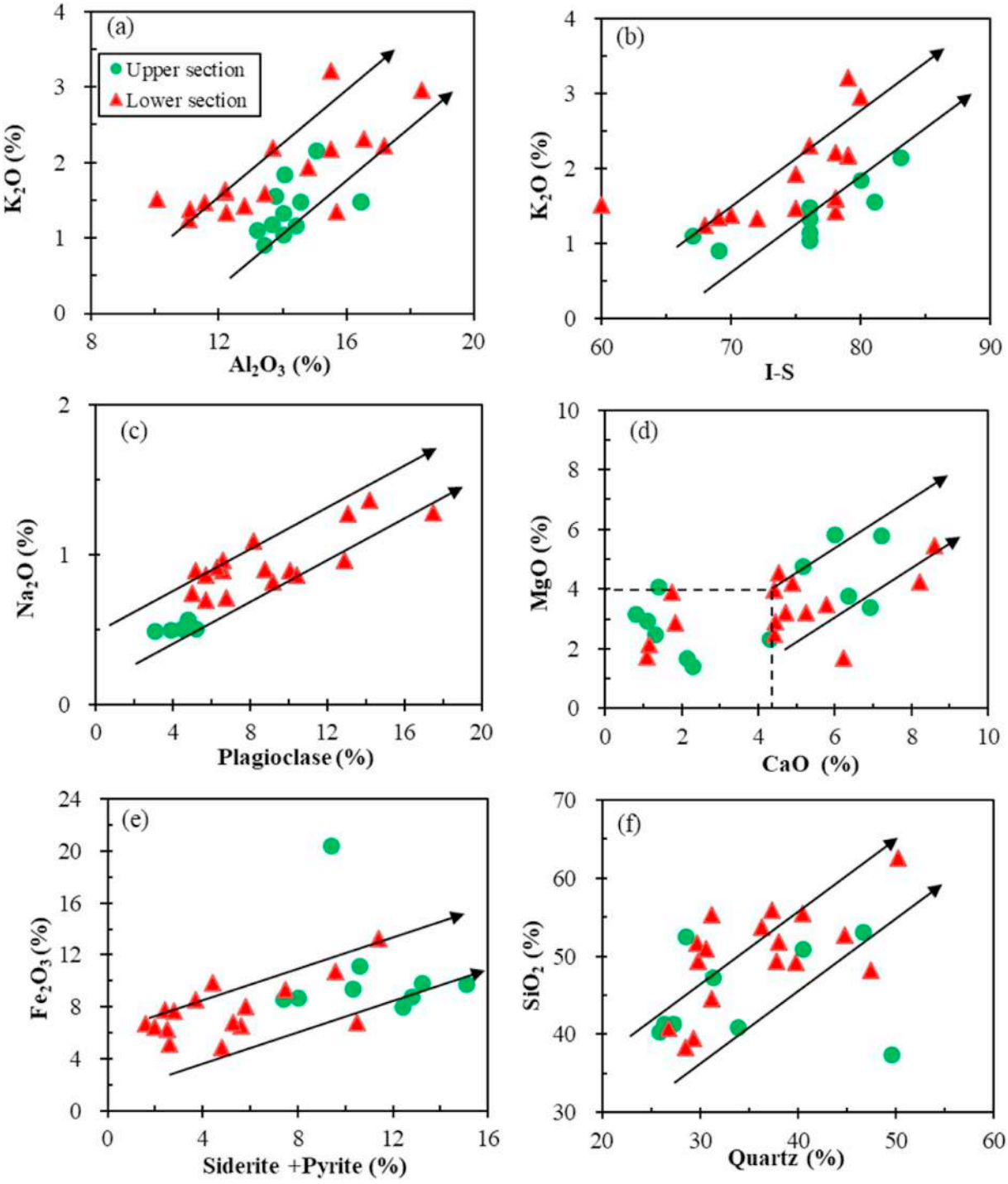

Fig. 5. Bivariate plots of major elements and minerals for the Es_4 shales.

probably more suitable than ICV to evaluate weathering degree in this study, as excluding the influence of CaO and MgO from carbonate, and Fe_2O_3 from pyrite and siderite. All the shales have K_2O/Al_2O_3 ratios ranging from 0.07 to 0.21. The upper section has lower K_2O/Al_2O_3 ratios (0.07–0.14, with a mean value of 0.1) than those from the lower section (0.09–0.21, with a mean value of 0.13, Table 2). The increasing K_2O/Al_2O_3 ratios in the deeper section probably relate to the decreasing clay minerals contents and increasing plagioclase contents (Fig. 3a and b).

In order to indicate the degree of chemical weathering, conversion degrees of feldspar to clay minerals are employed and are expressed by the CIA (Chemical Index of Alteration, Nesbitt and Young, 1982; Zhou et al., 2015). CIA is calculated by the following formula: CIA = $[Al_2O_3/(Al_2O_3 + CaO^* + Na_2O + K_2O)] \times 100$ (all in molar contents). The shales in the Es_4 yield CIA values varying from 37.46 to 82.34 with average of 63.69 (Table 2). CIA in the upper section (average of 67.35) is slightly higher than that of the lower section (average of 61.11).

Destruction degree of plagioclase, quantified by PIA (Plagioclase Index of Alteration), can be used to assess parental detritus weathering and elements redistribution during diagenesis (Fedo et al., 1995). PIA is calculated by $100 \times (Al_2O_3 - K_2O)/(Al_2O_3 + CaO^* + Na_2O - K_2O)$ (all in molar contents). The Es_4 shales yield PIA values locating between 34.13 and 92.89 with a mean value of 69.48 (Table 2). PIA in the upper section (average of 72.75) is slightly higher than that in the lower

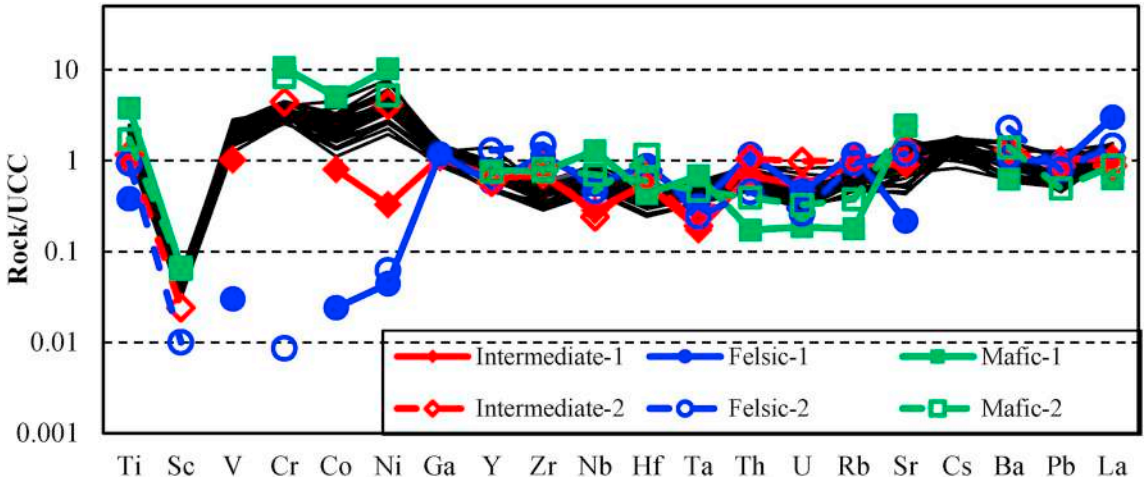

Fig. 6. Distribution patterns of trace elements of the Es_4 shales normalized by the UCC according to Taylor and McLennan (1985). Intermediate-1 and felsic-1 are from the Mesozoic volcanic lavas in the Liaohe Depression (northeast of the NCC) locating on the south of this study area (Sun et al., 2017). Intermediate-2, felsic-2 and mefic-2 are collected from the Mesozoic volcanic rocks in the northeast NCC (Yang and Li, 2008). Mefic-1 is collected from the Cenozoic basalts lying in the Jiyang Depression (Li et al., 2014).

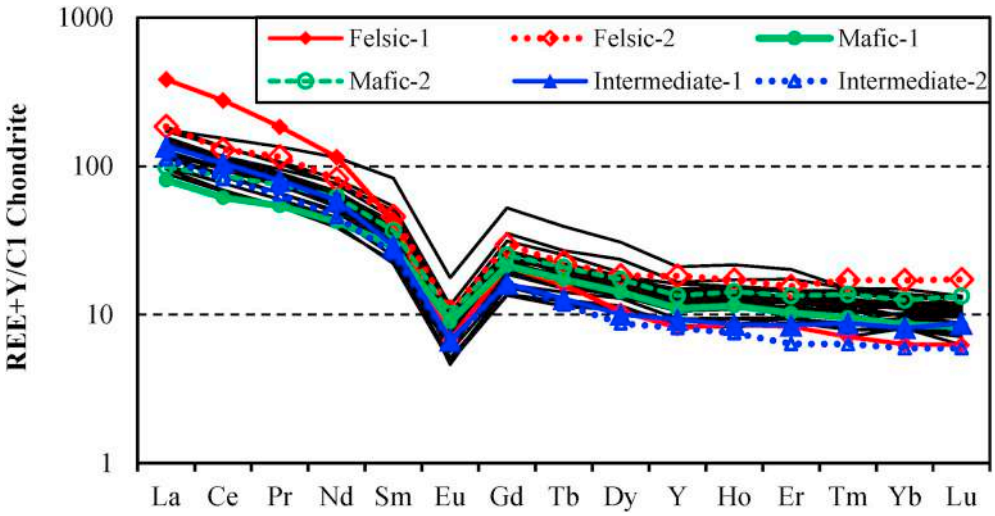

Fig. 7. C1-chondrite normalized REE + Y plots of the Es_4 shales. Intermediate rocks, felsic rocks and mafic rocks are the same samples presented in Fig. 6. REE + Y of the C1-chondrite is from Anders and Grevesse (1989).

section (average of 67.17).

5. Discussion

Studies demonstrate that enrichment of early diagenetic minerals (authigenic carbonate and phosphorite) and organic matters in shales could change the contents of trace elements and REEs (Abanda and Hannigan, 2006). But, low permeability of shales confines the loss of trace elements unless large quantities of organic matter have converted into oil and gas (Abanda and Hannigan, 2006). Considering of the low content of CaO and P_2O_5 and low compositional maturity of the Es_4 shales, trace elements and REEs are probably still mainly controlled by silicates, and thus can reflect information about provenance, paleo-weathering and tectonic setting.

5.1. Provenance

Although major elements show a wide variation among these analyzed samples, trace elements and REEs have similar distributions (Figs. 6 and 7). This indicates a common source of detritus for the Es_4 shales. Distribution patterns of the UCC normalized trace elements of the Es_4 shales mimic those of the Mesozoic to Cenozoic mafic igneous rocks and intermediate igneous rocks rather than felsic igneous rocks (Fig. 6). On the UCC normalized trace elemental distribution patterns, big deviations of V, Cr, Co and Ni are observed between the Es_4 shales and the Mesozoic felsic igneous rocks located at the northeast NCC (North China Craton). Intermediate-2, so called the Mesozoic volcanic rock from the northeast NCC, has the most similar trace elements distribution pattern to the Es_4 shales. Thus, the source materials for the Es_4 shales probably are the Mesozoic intermediate igneous rocks developed at the northeast NCC.

Data of REE + Y are presented in Table 4 and their distribution patterns are normalized by the C1-chondrite in Fig. 7. All the Es_4 shales from different depths have similar C1-chondrite normalized REE + Y patterns. This indicates that there is only one type of detritus source for the Es_4 shales, or detritus from different types of parental rocks mixed uniformly. The Es_4 shales, intermediate igneous rocks, felsic igneous rocks and mafic igneous rocks show high $(La/Yb)_N$ ratios, flat HREE distributions and clear negative Eu_N/Eu^* anomalies. In contrast, the felsic-1 that represents the Mesozoic felsic igneous rocks at the northeast NCC have pronounced higher $(La/Yb)_N$ ratio (60.61) than that of the Es_4 shales (10.98–14.24, median in 12.45) (Table 4). No significant

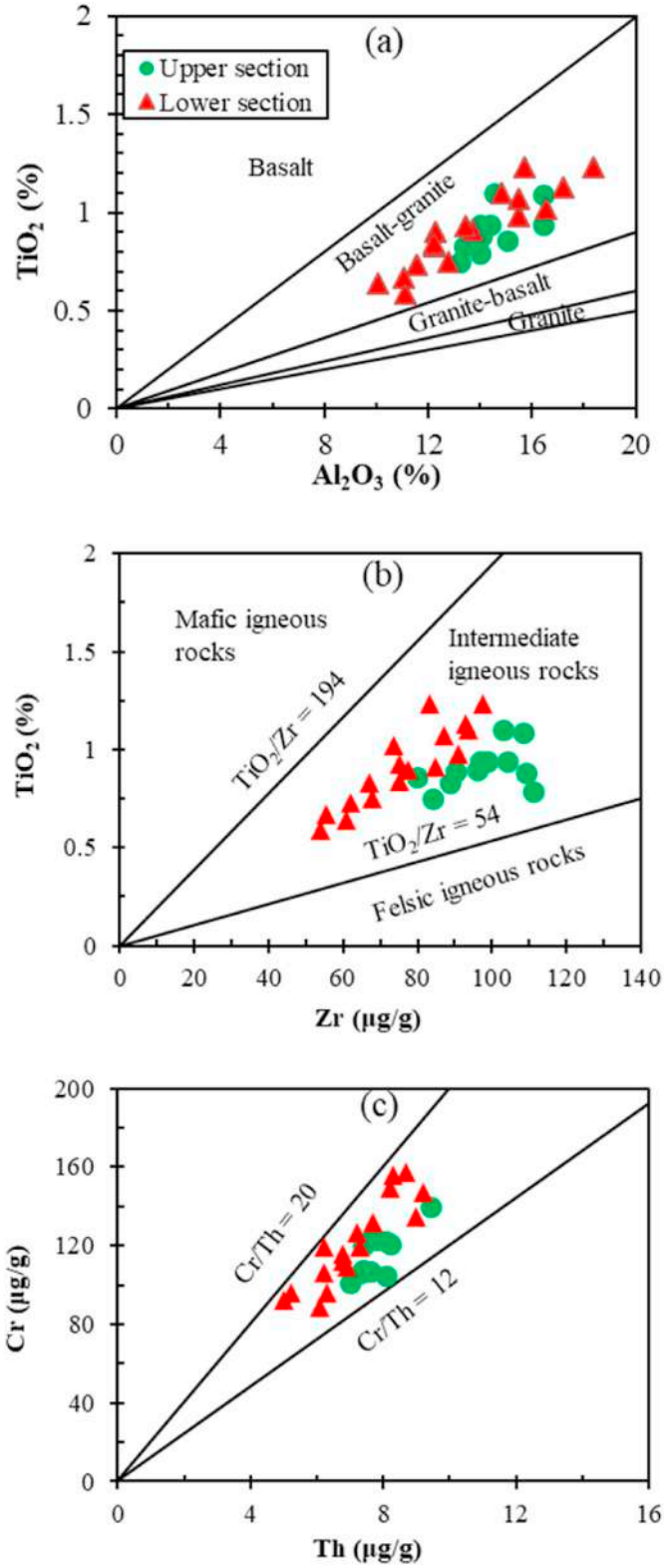

Fig. 8. Plots of (a) TiO_2 vs. Al_2O_3, (b) TiO_2 vs Zr, (c) Cr vs. Th for the Es_4 shales. Dividing lines in (a) and (b) are in accordance with Hayashi et al. (1997). Dividing lines in (c) are after Condie and Wronkiewicz (1990).

differences of Eu_N/Eu^* anomalies and $(Gd/Yb)_N$ is observed among the Es_4 shales, intermediate igneous rocks, felsic igneous rocks and mafic igneous rocks. The REE + Y distribution signatures suggest common parental materials for the Es_4 shales, which are intermediate to mafic igneous rocks developed during the Mesozoic to Cenozoic in the northeast NCC.

Alkali metal and alkali-earth metal elements such as Na, K, Ca, and Mg are more susceptible to weathering compared to immobile elements like Al, Ti, and Zr, and thus these immobile elements will be retained in the rocks during weathering processes (Harnois, 1988; Middleburg et al., 1988; Cox et al., 1995; Zhou et al., 2015). Therefore, ratios among Al, Ti and Zr of sediments are widely used to trace their source rocks (Zhou et al., 2015). Al_2O_3/TiO_2 weight ratios had been reported for mafic igneous rocks of 3–8, intermediate igneous rocks of 8–21, and felsic igneous rocks of 21–70 (Hayashi et al., 1997). The AlO_3/TiO_2 values of the Es_4 shales all fall in the range of 12.76–18.81 with an average value of 15.54 (Fig. 8a). This implies their parent materials are intermediate igneous rocks. TiO_2/Zr ratios of the Es_4 shales were also presented to indicate provenance, as Zr incline to reside in zircon because of its high resistance to chemical weathering, whereas Ti primarily reside in biotite and hornblende due to low resistance to chemical weathering (Tole, 1985; Zhou et al., 2015). As decreasing of SiO_2 contents, TiO_2/Zr ratios increase from less than 55 for felsic igneous rocks, between 55 and 195 for intermediate igneous rocks, and more than 200 for mafic igneous rocks (Hayashi et al., 1997). TiO_2/Zr ratios of the Es_4 shales locate between 71.2 and 147.8 with a mean value of 108.7, which is covered by the intermediate igneous rocks (Fig. 8b). Immobile elements, La and Th are mainly hosted by felsic igneous rocks, and Sc, Co, and Cr are largely hosted by mafic igneous rocks (Wronkiewicz and Condie, 1989, 1990). Thus Cr/Th ratio is very useful to differentiate debris source. According to Condie and Wronkiewicz (1990), relative consistent Cr/Th ratios ranging from 12.96 to 19.91 in the Es_4 shales also support a homogeneous source and efficient mixing of intermediate igneous rocks (Fig. 8c).

5.2. Paleo-weathering

Alkalis are gradually leached out of detritus as increasing transformation of feldspars to clay minerals, resulting in increasing ratios of Al to Ca, Na and K (Nesbitt and Young, 1982). K_2O/Al_2O_3 ratio of feldspars is greater than 0.3. Clay minerals usually present K_2O/Al_2O_3 ratios near zero, for example montmorillonite and kaolinite (Cox et al., 1995). K_2O/Al_2O_3 ratios in the Es_4 shales range from 0.07 to 0.21 with a mean value of 0.12 (Table 2), which demonstrate source rocks suffered a chemical weathering from moderate to intense. This conclusion from major oxides of the Es_4 shales in agreement with the warm, semi-humid climate at the stage of the Es_4 according to Liu et al. (2011) and Xia et al. (2015).

CIA and PIA, both calculated by molar contents of Al_2O_3, CaO*, Na_2O and K_2O to indicate destruction degree of feldspar, show a positive linear correlation (Fig. 9a). A negative trend of CIA vs. ICV is also presented in Fig. 9b, as they respectively express ratios of stable/unstable oxides and unstable/stable oxides. Comparing with CIA and PIA, contents of Fe_2O_3*, MgO*, MnO and TiO_2 are added to calculate ICV, that is the reason for the weak correlation between CIA and ICV in Fig. 9b. The bivariate relationships of CIA vs. PIA and CIA vs. ICV indicate that the three indexes are reliable to evaluate weathering degree (Fig. 9a and b). ICV values decrease with increasing compositional maturity, as mature mudstones contain enriched contents of clay minerals. Due to decreasing of Al_2O_3 contents, ICV values are < 0.12 in clay minerals (like montmorillonite and illite), 0.13–5 in feldspars and biotite, 5–20 in amphibole, and 20–300 in pyroxene (Cox et al., 1995). All the Es_4 shales have similar ICV values and vary from 0.20 to 1.80 that belonging to the range of clay minerals and feldspars. Medium PIA values of the Es_4 shales (34.13–92.89, average of 69.48) are in agree with ICV values, which indicates variable weathering degree from moderate to intense.

Compared to rhyolites and basalts, andesite is plotted on the weathering line of the Es_4 shales (Fig. 9c). Therefore, intermediate igneous rocks represented by andesite should be the most possible source for the Es_4 shales. The Es_4 shales are most plotted on or near the ideal

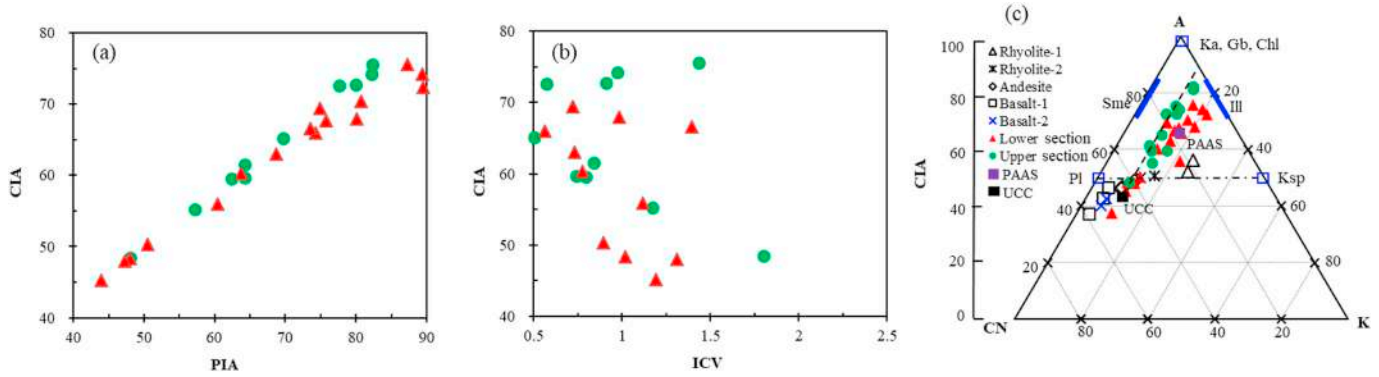

Fig. 9. (a) Relation between PIA and CIA. (b) Relation between ICV and CIA. (c) The A-CN-K plots (Nesbitt, 2003) of the Es_4 shales. Data collected from the UCC, PAAS and various igneous rocks are provided for comparison. Dashed line in the A-CN-K is the ideal trajectory for weathering. The dotted line represents feldspar join. Note that these igneous rocks used for comparison are same with that used in Figs. 6 and 7. A = Al_2O_3; CN = (CaO^* + Na_2O); K = K_2O (molar proportion). CaO^* = CaO content in silicate minerals. Mineral compositions: Pl = plagioclase; Ka = kaolinite; Ksp = K-feldspar; Chl = chlorite; Gb = gibbsite.

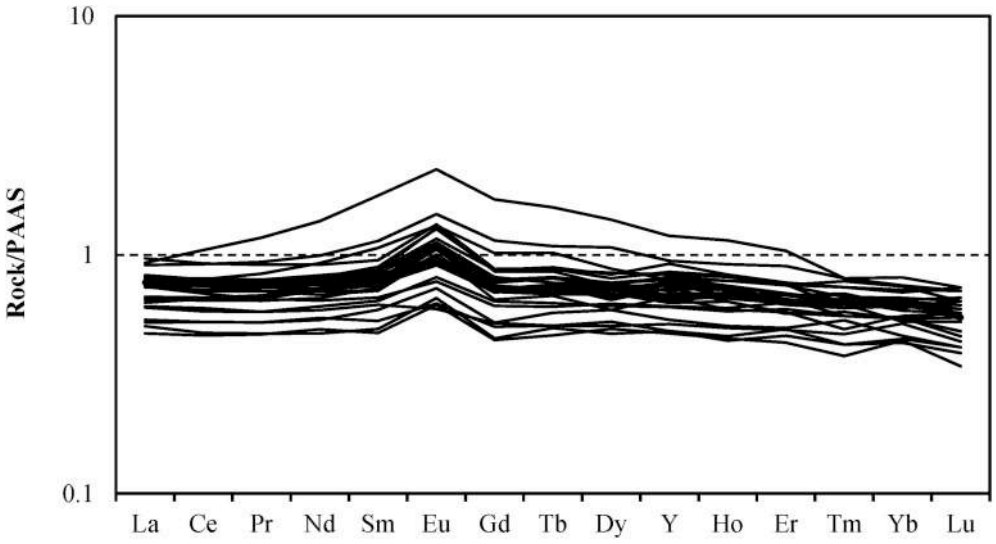

Fig. 10. PAAS-normalized rare earth element and Yttrium (REE + Y) plots for the Es4 shales. REE + Y of the PAAS is from Pourmand et al. (2012).

weathering line, and show relatively moderate and wider estimated CIA values (40–80, median in 60, Fig. 9c). The calculated CIA values (37.46–82.34, median in 63.69) are similar to the estimated ones. The CIA value for feldspars is 50, and for secondary clay minerals is 70–100 (Nesbitt and Young, 1982). Both calculated and estimated CIA values demonstrate a mild and variable weathering for parent materials, even though negligible differences exist between calculated and estimated CIA. This indicates an intense erosion and non-steady state weathering under a relatively active tectonic setting. This is also consistent with the warm, semi-humid paleo-climate and active tectonic setting during the Es_4 period.

5.3. Paleo-sedimentation environment

5.3.1. Paleo-redox conditions

It is common that dissolved sulfate in marine or lake is reduced to H_2S by bacterial sulfate reduction represented by the simple reaction:

$$2CH_2O + SO_4^{2-} \rightarrow H_2S + 2HCO_3^-,$$

where sedimentary organic matter is represented by the idealized formula CH_2O (Westrich, 1983). Pyrite is formed when H_2S react with Fe^{2+} and detected in many black shales that deposited in reducing water column. Therefore, pyrite is extensively employed as a sensitive redox indicator (Jones and Manning, 1994; Zhou et al., 2015; Qiu et al., 2015; Tao et al., 2016). Content of Pyrite in the black shale is controlled by content of S^{2-} and Fe^{2+}, and only show positive correlation with organic C when constant proportion of originally deposited organic matter is used to form pyrite (Berner, 1984). Pyrite in the Es_4 shales lies between 1.7% and 12.6% with an average of 4.4% whose content is comparable to that of the Chang 7 shales in the Ordos Basin (Qiu et al., 2015) and the Upper Paleocene shale in Siri Canyon (Zhou et al., 2015) that were deposited under dysoxic or anoxic environment. The Es_4 shales show organic C content ranging from 1.59% to 7.50% with an average of 4.91% and have obviously lower S/C ratios compared with the normal marine regression line (Fig. 11a). These lower S/C ratios are common in non-marine fresh water according to Berner and Raiswell (1984), which indicate an ancient lake environment of the Es_4 shales. Formation of pyrite in the Es_4 shales was possibly restricted by dissolved sulfate in the ancient lake, instead of available iron from the sediments.

U/Th, V/Cr and Ni/Co have been suggested as redox indicators, as U, V and Ni will be incorporated into sediments in their reduced valences (Jones and Manning, 1994; Qiu et al., 2015; Zhang et al., 2017). Calculated U/Th (0.11–0.25), V/Cr (0.80–1.46) and Ni/Co (2.42–4.40) of the Es_4 shales fall in the range of oxic environment presented by Jones and Manning (1994), which is contrary to the conclusion demonstrated by TOC and pyrite. We consider these absolute ratios of U/Th, V/Cr and Ni/Co are inherited from their parental rocks rather than reflecting the paleo-redox conditions. Whereas, positive linear relationship between TOC and U/Th indicates that U/Th tendency can

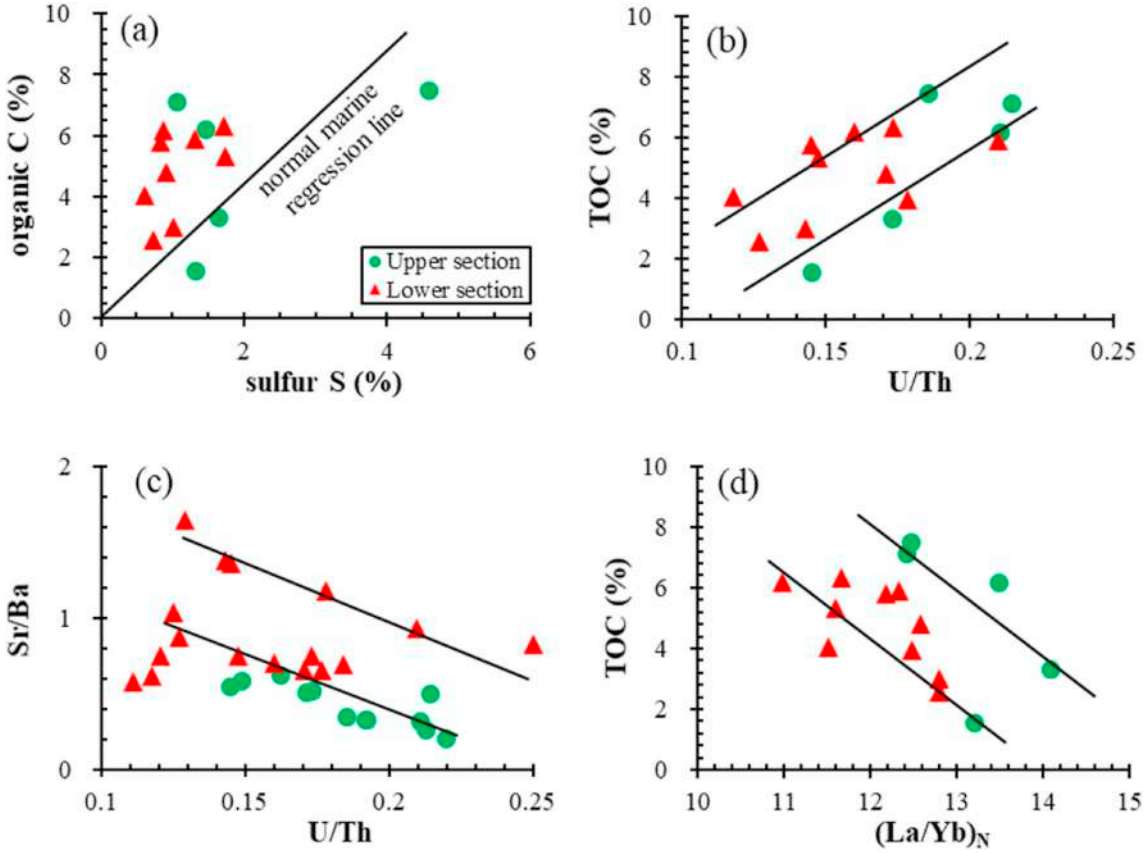

Fig. 11. Correlation of (a) TOC and pyrite; (b) TOC and U/Th; (c) Sr/Ba and U/Th; (d) TOC and $(La/Yb)_N$.

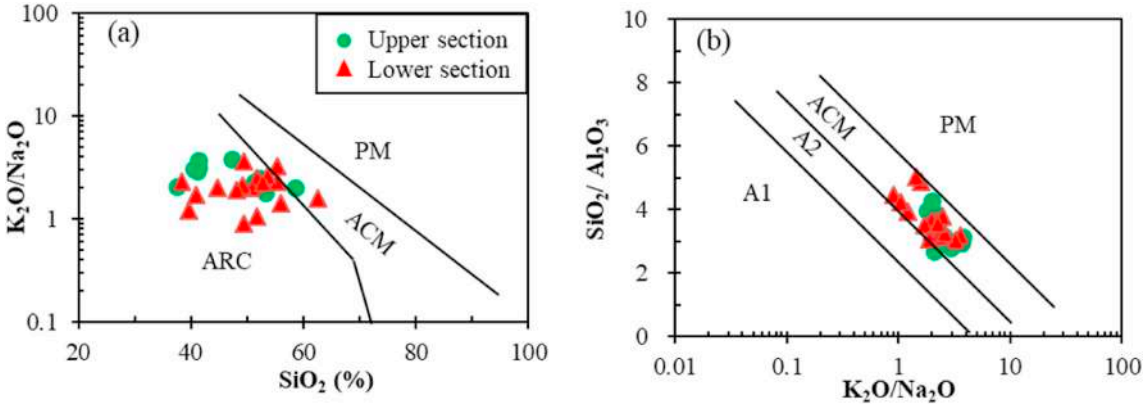

Fig. 12. Plots of (a) SiO_2 vs. K_2O/Na_2O and (b) SiO_2/Al_2O_3 vs. K_2O/Na_2O of the Es_4 shale rocks in the Damintun Sag for discrimination of tectonic setting. Boundaries for different tectonic settings in agreement with Roser and Korsch (1986). Abbreviation: ARC, oceanic island arc margin; ACM, active continental margin; PM, passive margin; A1, arc setting; A2, evolved arc setting.

still reflect variation of redox degree (Fig. 11b). Low contents of TOC in some Es_4 shales may be diluted by detritus influx from intermediate rocks with low U/Th ratios.

5.3.2. Paleo-salinity

Sr/Ba ratios are often used to study paleo-salinity in sedimentary depositional environments (Zhang et al., 2017; Zhang et al., 2018). Usually, fresh water has Sr/Ba ratio less than 1, and brackish water show Sr/Ba ratio higher than 1. Sr/Ba ratios of the Es_4 shales range from 0.21 to 1.64 with a mean value of 0.71, which indicates variable and low water salinity. A negative correlation exists between Sr/Ba and U/Th (Fig. 11c). Higher Sr/Ba ratios coincide with lower U/Th ratios possible suggest some shale deposited in shallower evaporated water with more oxygen. High-level terrigenous influx, raised water level and diluted water salinity, probably lead to the lower Sr/Ba ratios, and corresponding higher U/Th ratios support reducing oxygen content in deeper water.

5.3.3. Paleo-influx rate

Sediments deposited in anoxic deeper water are generally enriched in LREE (Light Rare Earth Element), and HREE (Heavy Rare Earth Element) are enriched in oxic surface water (Elderfield and Greaves, 1982). Besides, REEs signature is either influenced by their source rocks. $(La/Yb)_N$ ratios are calculated to express the fractionation degree between LREE and HREE. $(La/Yb)_N$ ratios of the Es_4 shales are negatively correlated with TOC and range from 10.98 to 14.24 with an

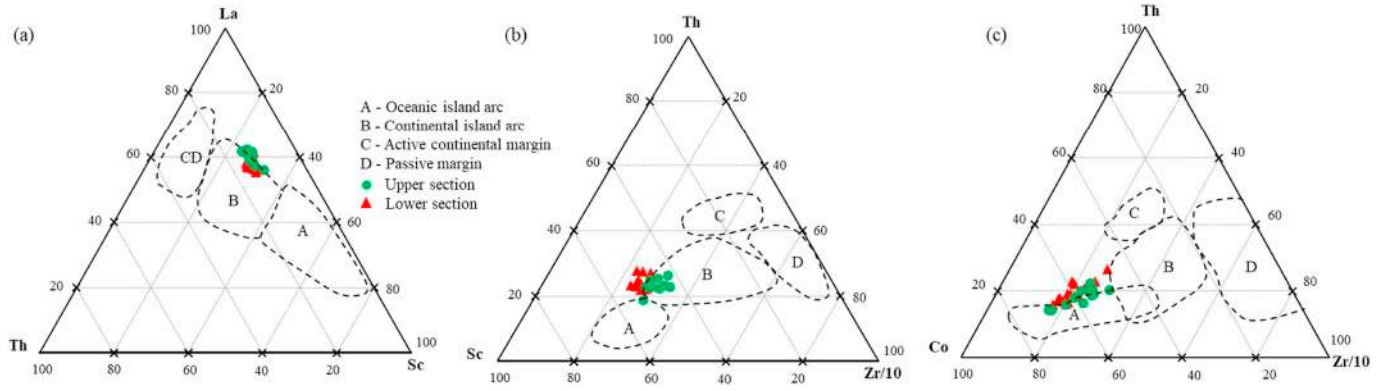

Fig. 13. (a) La - Th - Sc discriminatory plot, (b) Th - Sc - Zr/10 discriminatory plot and (c) Th - Co - Zr/10 discriminatory plot for shale samples after Bhatia and Crook (1986). Abbreviation: A, oceanic island arc; B, continental island arc; C, active continental margin; D, passive margin.

average of 12.45 that is similar to their source rocks (Table 3, Fig. 11d). This indicate $(La/Yb)_N$ ratios of the Es_4 shales reflect more information about parental rocks rather than redox conditions. Organic matters can be diluted by highly terrigenous influx rate, and consequently result in lower content of TOC in some Es_4 shales.

5.4. Tectonic setting

Plots of K_2O/Na_2O vs. SiO_2 were employed to defined tectonic settings such as oceanic island arc (ARC), passive margin (PM) and active continental margin (ACM) (Roser and Korsch, 1986). Bivariate plots of SiO_2/Al_2O_3 vs. K_2O/Na_2O were either used to indicate tectonic settings (Roser and Korsch, 1986). Most samples from the Es_4 shales fall in the area of ARC in Fig. 12a and ACM in Fig. 12b. Na_2O, the most active oxide in major rock-forming minerals, can vary rapidly during weathering, sedimentation, diagenetic and metamorphic processes (Zhou et al., 2015). And this probably relates to the different results deciphered in Fig. 12a and b. Therefore, applying K_2O/Na_2O ratios to reconstruct tectonic setting in Fig. 12 should be carefully reconsidered. If Na_2O depletion is pronounced due to these post-depositional processes, the original K_2O/Na_2O values should be smaller. Compared to their initial positions, the Es_4 shales should have been plotted downward in Fig. 12a and left in Fig. 12b. Then, most of the Es_4 shales defining as active continental margin would like to be more typical of ARC in Fig. 12a and ACM to A2 in Fig. 12b.

Immobile trace elements in detritus like La, Ce, Nd, Th, Zr, Hf, Nb, Ti, and Sc are sustained during weathering, denudation, transport and sedimentation, so they are employed to reconstruct tectonic setting (Taylor and McLennan, 1985; McLennan, 1989). On the tri-variate discrimination plots of La-Th-Sc and Th-Sc-Zr/10, most of the Es_4 shales fall on the border or in the areas defined as continental island arc (Fig. 13a and b). Whereas, data are relatively scatter and close to oceanic island arc on the Th-Co-Zr/10 discrimination plot (Fig. 13c). Rimstidt et al. (2017) reported that La, Th Sc and Co are slightly depleted in carbonaceous black shale compared to normal shale, Co content is also correlated with pyrite content strongly, whereas Zr is barely influenced. Carbonate and pyrite are both observed in the Es_4 shales. Therefore, Co is probably more depleted than La, Th and Sc in these shales. In this respect, the Es_4 shales most plotted outside of A and B should have been plotted closer to oceanic island arc in Fig. 13c. Therefore, the Es_4 shale show a tectonic setting of oceanic island arc or continental island arc.

6. Conclusion

Source detritus for the Es_4 shales in the Damintun Sag are mainly from the Mesozoic and Cenozoic intermediate igneous rocks developed at the northeast NCC. Weathering proxies, K_2O/Al_2O_3, ICV, PIA and CIA, imply that detritus underwent moderate to intense weathering in a warm, semi-humid paleo-climate during the Es_4 period. Organic matters of the Es_4 shale are preserved in a deep and anoxic water column, and can be diluted by the relatively fast detritus influx due to active tectonic movement under a tectonic setting of oceanic/continental island arc.

Acknowledgments

This research is supported by Open Fund (NEPUME-kfjj-006) of Key Laboratory of Continental Shale Hydrocarbon Accumulation and Efficient Development (Northeast Petroleum University), Ministry of Education of China and the National Natural Science Foundation of China (No. 41972156). Thanks also to the Scientific Foundation Program for Young Scholars in the Northeast Petroleum University (2018QNL-41). A lot of thanks should be given to the PetroChina Liaohe Oilfield Company for supporting this study, and to the editors and anonymous reviewers for their valuable suggestions to make this paper more deliberate and better understood.

Appendix A. Supplementary data

Supplementary data to this article can be found online at https://doi.org/10.1016/j.marpetgeo.2019.09.002.

References

Abanda, P.A., Hannigan, R.E., 2006. Effect of diagenesis on trace element partitioning in shales. Chem. Geol. 230, 42–59.
Anders, E., Grevesse, N., 1989. Abundances of the elements: meteoritic and solar. Geochem. Cosmochim. Acta 53, 197–214.
Balaram, V., Rao, T.G., 2003. Rapid determination of REEs and trace elements in geological samples by microwave acid digestion and ICP-MS. Atom. Spectrosc. Norwalk Conn. 24, 206.
Berner, R.A., 1984. Sedimentary pyrite formation: an update*. Geochem. Cosmochim. Acta 48, 605–615.
Berner, R.A., Raiswell, R., 1984. C/S method for distinguishing freshwater from marine sedimentary rocks. Geology 12, 365–368.
Bhatia, M.R., Crook, K.A., 1986. Trace element characteristics of graywackes and tectonic setting discrimination of sedimentary basins. Contrib. Mineral. Petrol. 92, 181–193.
Condie, K.C., Wronkiewicz, D.J., 1990. The Cr/Th ratio in Precambrian pelites from the Kaapvaal Craton as an index of craton evolution. Earth Planet. Sci. Lett. 97, 256–267.
Cox, R., Lowe, D.R., Culler, R.L., 1995. The influence of sediment recycling and basement composition on evolution of mudrock chemistry in the southwestern United States. Geochem. Cosmochim. Acta 59, 2919–2940.
Cullers, R.L., 1994. The controls on the major and trace element variation of shales, siltstones, and sandstones of Pennsylvanian-Permian age from uplifted continental blocks in Colorado to platform sediment in Kansas, USA. Geochem. Cosmochim. Acta 58, 4955–4972.
Elderfield, H., Greaves, M.J., 1982. The rare earth elements in seawater. Nature 296, 214–219.
Espitalié, J., Deroo, G., Marquis, F., 1985. La pyrolyse Rock-Eval et ses applications, Partie II. Rev. Inst. Fr. Du. Pétrole 40, 755–784.
Fedo, C.M., Wayne Nesbitt, H., Young, G.M., 1995. Unraveling the effects of potassium

metasomatism in sedimentary rocks and paleosols, with implications for paleoweathering conditions and provenance. Geology 23, 921.
Ghosh, S., Sarkar, S., 2010. Geochemistry of Permo-Triassic mudstone of the Satpura Gondwana basin, central India: Clues for provenance. Chem. Geol. 277, 78–100.
Harnois, L., 1988. The CIW index: a new chemical index of weathering. Sediment. Geol. 55, 319–322.
Hayashi, K.I., Fujisawa, H., Holland, H.D., Ohmoto, H., 1997. Geochemistry of ~1.9 Ga sedimentary rocks from northeastern Labrador, Canada. Geochem. Cosmochim. Acta 61, 4115–4137.
Huang, H., Larter, S.R., Love, G.D., 2003. Analysis of wax hydrocarbons in petroleum source rocks from the Damintun depression, eastern China, using high temperature gas chromatography. Org. Geochem. 34, 1673–1687.
Jones, B., Manning, D.A.C., 1994. Comparison of geochemical indices used for the interpretation of palaeoredox conditions in ancient mudstones. Chem. Geol. 111, 111–129.
Liu, C.H., Wei, W.Y., Ren, Z.Y., Wang, Y., Qu, R.T., Yang, J.L., Qi, Y.M., 2011. The palaeontological assemblage from the Es4 of the Bodong depression in the Bohai Sea and its significance. Acta Micropalacontol. Sin. 28 (3), 316–323.
Li, H.Y., Huang, X.L., Guo, H., 2014. Geochemistry of Cenozoic basalts from the Bohai Bay Basin: implications for a heterogeneous mantle source and lithospheric evolution beneath the eastern north China craton. Lithos 196–197, 54–66.
McLennan, S.M., 1989. Rare earth elements in sedimentary rocks: influence of provenance and sedimentary processes. Rev. Mineral. Geochem. 21, 169–200.
Middleburg, J.B., Van der Weijden, C.H., Woittiez, J.R.W., 1988. Chemical processes affecting the mobility of major, minor and trace elements during weathering of granitic rocks. Chem. Geol. 68, 253–273.
Nesbitt, H.W., Young, G.M., 1982. Early Proterozoic climates and plate motions inferred from major element chemistry of lutites. Nature 299, 715–717.
Nesbitt, H.W., 2003. Petrogenesis of siliciclastic sediments and sedimentary rocks. In: Lentz, R.D. (Ed.), Geochemistry of Sediments and Sedimentary Rocks: Evolutionary Considerations to Mineral-Deposit-Forming Environments. Geological Association of Canada, pp. 39–51 GEOText 4.
Pourmand, A., Dauphas, N., Ireland, T.J., 2012. A novel extraction chromatography and MC-ICP-MS technique for rapid analysis of REE, Sc and Y: revising CI-chondrite and Post-Archean Australian Shale (PAAS) abundances. Chem. Geol. 291, 38–54.
Qiu, X., Liu, C., Mao, G., Deng, Y., Wang, F., Wang, J., 2015. Major, trace and platinum-group element geochemistry of the Upper Triassic nonmarine hot shales in the Ordos basin, Central China. Appl. Geochem. 53, 42–52.
Rimstidt, J.D., Chermak, J.A., Schreiber, M.E., 2017. Processes that control mineral and element abundances in shales. Earth Sci. Rev. 171, 383–399.
Roser, B.P., Korsch, R.J., 1986. Determination of tectonic setting of sandstone-mudstone suites using SiO_2 content and K_2O/Na_2O ratio. J. Geol. 94, 635–650.
Sun, J., Liu, Z., Zhang, S., Li, X., Qi, J., 2017. Large-scale removal of lithosphere underneath the north China craton in the early Cretaceous: geochemical constraints from volcanic lavas in the Bohai Bay Basin. Lithos 292–293, 69–80.
Tao, S., Shan, Y., Tang, D., Xu, H., Li, S., Cui, Y., 2016. Mineralogy, major and trace element geochemistry of Shichanggou oil shales, Jimusaer, Southern Junggar Basin, China: implications for provenance, palaeoenvironment and tectonic setting. J. Pet. Sci. Eng. 146, 432–445.
Taylor, S.R., McLennan, S.M., 1985. The Continental Crust: its Composition and Evolution. Blackwell, pp. 312.
Tole, M.P., 1985. The kinetics of dissolution of zircon ($ZrSiO_4$). Geochem. Cosmochim. Acta 49, 453–458.
Wang, Y., Cheng, S.H., 2012. Field relation, geochemistry and origin of the Xinglonggou volcanic rocks in Beipiao area, Liaoning Province (China): reappraisal on the foundering of lower continental crust of North China Craton. J. Asian Earth Sci. 47, 35–50.
Westrich, J.T., 1983. The Consequences and Controls of Bacterial Sulfate Reduction in Marine Sediments. Ph.D. dissertation. Yale University 530 p.
Wronkiewicz, D.J., Condie, K.C., 1989. Geochemistry and provenance of sediments from the Pongola Supergroup, South Africa: evidence for a 3.0-Ga-old continental craton. Geochem. Cosmochim. Acta 53, 1537–1549.
Wronkiewicz, D.J., Condie, K.C., 1990. Geochemistry and mineralogy of sediments from the Ventersdorp and Transvaal Supergroups, South Africa: cratonic evolution during the early Proterozoic. Geochem. Cosmochim. Acta 54, 343–354.
Xia, X.F., Zhang, N., Yu, J.X., Yi, C., 2015. Eocene-oligocene palynology and biostratigraphy correlation in the Nanpu sag, Bohai Bay Basin. Acta Micropalacontol. Sin. 32 (3), 269–284 (In Chinese).
Yang, W., Li, S., 2008. Geochronology and geochemistry of the mesozoic volcanic rocks in Western Liaoning: implications for lithospheric thinning of the north China craton. Lithos 102, 88–117.
Zhou, L., Friis, H., Poulsen, M.L.K., 2015. Geochemical evaluation of the late Paleocene and early Eocene shales in Siri Canyon, Danish-Norwegian basin. Mar. Pet. Geol. 61, 111–122.
Zhang, S., Liu, C., Liang, H., Wang, J., Bai, J., Yang, M., Liu, G., Huang, H., Guan, Y., 2018. Paleoenvironmental conditions, organic matter accumulation, and unconventional hydrocarbon potential for the Permian Lucaogou Formation organic-rich rocks in Santanghu Basin, NW China. Int. J. Coal Geol. 185, 44–60.
Zhang, W., Yang, W., Xie, L., 2017. Controls on organic matter accumulation in the Triassic Chang 7 lacustrine shale of the Ordos Basin, central China. Int. J. Coal Geol. 183, 38–51.